PNAS RESEARCH ARTICLE | APPLIED PHYSICAL SCIENCES

Odd viscosity-induced Hall-like transport of an active chiral fluid

Xin Lou[a,b,c,d,1], Qing Yang[a,b,c,d,1], Yu Ding[a,b,c], Peng Liu[a,b,c,d], Ke Chen[a,b,c,e], Xin Zhou[a,b,c,d,2], Fangfu Ye[a,b,c,d,e,2], Rudolf Podgornik[a,b,c,d,f,2], and Mingcheng Yang[a,b,c,e,2]

Edited by Steve Granick, Institute for Basic Science, Ulju-gun, Ulsan, Republic of Korea (South); received January 24, 2022; accepted August 30, 2022

Broken time-reversal and parity symmetries in active spinner fluids imply a nondissipative "odd viscosity," engendering phenomena unattainable in traditional passive or active fluids. Here we show that the odd viscosity itself can lead to a Hall-like transport when the active chiral fluid flows through a quenched matrix of obstacles, reminiscent of the anomalous Hall effect. The Hall-like velocity depends significantly on the spinner activity and longitudinal flow due to the interplay between odd viscosity and spinner–obstacle collisions. Our findings underscore the importance of odd viscosity in active chiral matter and elucidate its essential role in the anomalous Hall-like effect.

active chiral matter | Hall-like flow | odd viscosity | collective behavior

Significance

Unlike common viscosities associated with dissipation, a nondissipative "odd viscosity," producing transverse stresses, can emerge in isotropic fluids with broken time-reversal and parity symmetries, e.g., electronic Hall systems and chiral active fluids consisting of self-driven spinners. The odd viscosity has been repeatedly reported to importantly correct the Hall conductance of electronic systems, but its effects on mass transport of active spinner fluids have not been explored. Here, we show that the odd viscosity itself is sufficient to generate a transverse mass transport when the spinner fluid flows through a quenched matrix of obstacles, reminiscent of the anomalous Hall effect. This finding significantly advances our understanding of the essential role of odd viscosity in the mass transport of chiral active matter.

Active chiral matter consists of self-driven circle swimmers and/or spinners (1, 2), which are ubiquitous in nature and can be straightforwardly realized in the laboratory. Prominent examples range from rotating microorganisms (3–8), to synthetic colloidal rotors (9–18), to oscillating chiral grains (19–22). The active chiral systems are intrinsically out of equilibrium and break both time-reversal and parity symmetries. Remarkably, a two-dimensional active chiral fluid composed of interacting spinners has been recently shown to support a spontaneous topologically protected edge flow (20–24) and to possess a nondissipative momentum transport coefficient dubbed "odd viscosity" or "Hall viscosity" (25–31). Due to these intriguing and unique features, the active spinner system is stirring up fundamental theoretical interest.

As edge flow and odd viscosity are also important in electronic quantum-Hall systems (32–38), the active spinner fluid and the electronic quantum-Hall fluids thus share some fundamental physical features. Moreover, in analogy with the spin–spin and spin–orbital couplings in electronic systems, the active spinners can similarly couple via interparticle tangential interactions. As the active spinner fluid spontaneously breaks time-reversal and parity symmetries without any externally applied field, it acts more like an active counterpart of the anomalous Hall system (39–42), where the symmetries are broken by magnetization and spin–orbit coupling, rather than the Hall system, where the symmetries are broken by an external magnetic field. These apparent similarities inspired us to inquire whether the active spinner fluid may exhibit a Hall-like flux when it is driven through a matrix of impurities with quenched positions. The existence of such a flux would be related to the anomalous Hall effect in ferromagnetic conductors carrying a longitudinal current (43), where charge carriers create a Hall voltage by being forced toward the transverse side of the conductor in the absence of a magnetic field. Despite great progress on the anomalous Hall effect since its discovery (44), its understanding is still incomplete (41–43) and physical analogies from the active chiral matter dynamics can add important insights into the properties of these systems.

Here, by simulation and by analytical theory, we study transport behavior of a two-dimensional (2D) active spinner fluid externally driven to flow past a matrix of frozen obstacles that mimics the impurities in an anomalous Hall system. We find that the active chiral fluid exhibits a distinct transverse Hall-like flux perpendicular to the external driving force. The transverse transport occurs in both ordered and disordered obstacle backgrounds, and its velocity depends significantly on the spinner activity as well as the longitudinal flow. We unambiguously clarify that the Hall-like effect originates from the odd viscosity-induced asymmetric stress distribution of the spinner fluid subjected to nonuniform shear. Our results thus further establish an interesting and important link between the active spinner fluid and the anomalous Hall system.

Results

A periodic box of dimension 130×130 contains a matrix of fixed disk-shaped obstacles of packing fraction ρ_{ob}, defined with respect to the total system space, and an ensemble of active spinners of packing fraction ρ, defined with respect to the obstacle free space (Fig. 1). Each spinner is modeled as a disk driven by a constant torque of magnitude T_d. Interspinner and spinner–obstacle interactions are of a short-ranged repulsive potential,

Author contributions: F.Y., R.P., and M.Y. designed research; X.L., Q.Y., Y.D., and X.Z. performed research; X.L., Q.Y., Y.D., P.L., K.C., X.Z., F.Y., R.P., and M.Y. analyzed data; and R.P. and M.Y. wrote the paper.

The authors declare no competing interest.

This article is a PNAS Direct Submission.

[1]X.L. and Q.Y. contributed equally to this work.

[2]To whom correspondence may be addressed. Email: xzhou@ucas.ac.cn, fye@iphy.ac.cn, podgornikrudolf@ucas.ac.cn, or mcyang@iphy.ac.cn.

This article contains supporting information online at https://www.pnas.org/lookup/suppl/doi:10.1073/pnas.2201279119/-/DCSupplemental.

Published October 10, 2022.

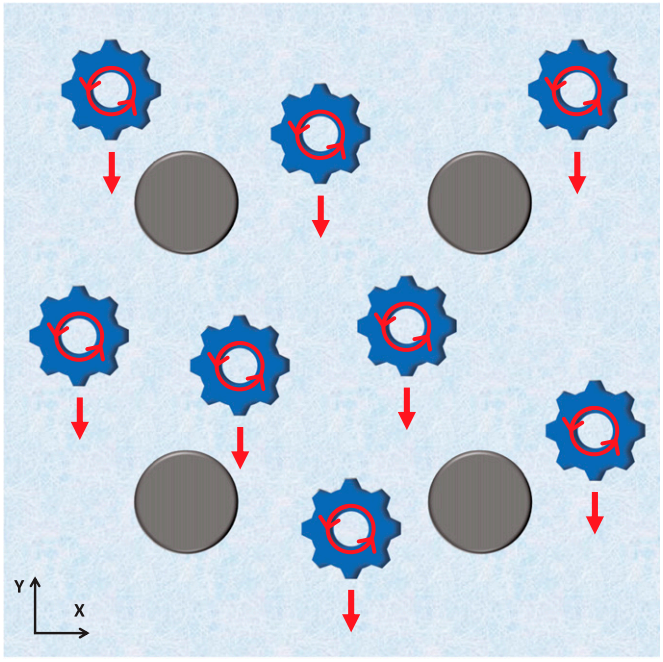

Fig. 1. Sketched spinner fluid crossing a matrix of frozen obstacles. The spinners rotating counterclockwise are represented by the blue gears, flowing under a uniform external force, and the gray smooth disks refer to the fixed obstacles.

$U(r) = 4\epsilon\left[\left(\frac{\sigma_s}{r}\right)^{48} - \left(\frac{\sigma_s}{r}\right)^{24}\right] + \epsilon$ for $r < 2^{1/24}\sigma_s$, with the diameter $\sigma_s = 2$ and $\epsilon = 1$. Additionally, different spinners also couple tangentially via a friction realized by the bounce-back collisions (22, 45) (*SI Appendix*). Unless specifically stated, the obstacles are frictionless. A uniform external force $\boldsymbol{G}$ is applied to the spinners that generates a longitudinal flow in the y direction. The spinner dynamics evolve via the Langevin equation, with the temperature $k_B T = 1$, and translational and rotational friction coefficients $\gamma_s = 100$ and $\gamma_r = \frac{1}{3}\sigma_s^2\gamma_s$ (see *SI Appendix* for full simulation details).

A. Simulation Results in Square Lattice Matrix of Obstacles. We first consider a square lattice matrix of obstacles with $\rho_{ob} = 0.074$ (lattice constant 6.5). After a transient relaxation, the randomly positioned spinners rotating counterclockwise develop a stationary transverse flux in the x direction, in addition to the downward longitudinal flow driven by the external force, as shown in Fig. 2 (see also the trajectories in *SI Appendix*). The transverse flow velocity increases with the driving torque and also with $G = |\mathbf{G}|$ in the parameter range under study. On the other hand, the longitudinal flow increases linearly with G as expected, showing only a slight increase with T_d. Moreover, for clockwise rotating spinners, the transverse flow is reversed (*SI Appendix*). One can speculate that the interparticle friction plays a crucial role in the emergence of the Hall-like flux, since otherwise the spin would completely decouple from other degrees of freedom. This becomes clear by noting that the frictionless spinner fluid exhibits a perfect symmetry with respect to the obstacles in the x direction.

A stationary Hall-like flow means that the active chiral fluid must experience a transverse driving force along the x direction, which can only be exerted by the fixed obstacles. An intuitive explanation of the transverse transport can be based on microscopic collisions, as sketched in Fig. 3*A*. Specifically, a longitudinal flow of spinners crossing a smooth obstacle suffers from a local shear roughly symmetric with respect to the obstacle center, where the spinner at the top of the obstacle moves downward more slowly than its left and right neighbors, due to its direct interaction with the obstacle. In this case, the collisions on the top side of the obstacle are much stronger than those on the bottom side. Such biased interparticle collisions, coupled to the counterclockwise spin and interparticle friction, affect the spinner–obstacle interactions in a left–right asymmetric manner (Fig. 3*A*), resulting in a net transverse force on the spinner fluid directed to the right.

In the following, we theoretically demonstrate that the spinner transverse flow arises exclusively from the odd viscosity. The odd viscosity is allowed in the 2D spinner fluid because time-reversal and parity symmetries are broken due to unidirectional spin (25, 29, 46, 47). It depends on the spinner activity and is an odd function of the spinner chirality (25, 26, 31). When shearing the fluid in one direction, the odd viscosity induces a momentum transfer in the perpendicular direction. It has been found that the odd viscosity can contribute a correction to the Hall conductivity in the electronic Hall systems (38, 48–53).

B. Hydrodynamic Theory. To clarify the mechanism of the Hall-like transport, we use a 2D continuum hydrodynamic theory developed for the active spinner fluid (20, 25, 26). For simplicity, we consider an incompressible, $\nabla \cdot \mathbf{v} = 0$, unconfined spinner fluid flowing around a single, fixed obstacle. The momentum of the spinner fluid obeys the Navier–Stokes-type equation,

$$\varrho(\partial_t + \mathbf{v}\cdot\nabla)\mathbf{v} = \nabla\cdot\boldsymbol{\sigma} - \Gamma\mathbf{v} + \mathbf{g}, \qquad [1]$$

with ϱ the mass density; Γ the environment translational friction coefficient, which is related to its single-particle counterpart by $\Gamma = \gamma_s n$ ($n = 4\rho/\pi\sigma_s^2$ the spinner number density); and $\mathbf{g} = \boldsymbol{G}n$ the external force density. Here, the stress tensor, $\boldsymbol{\sigma}$, has the form

$$\boldsymbol{\sigma} = -p\mathbf{I} + \eta[\nabla\mathbf{v} + (\nabla\mathbf{v})^T] + \eta_R\boldsymbol{\epsilon}(2\omega - \Omega) + \eta_o(\nabla\mathbf{v}^* + \nabla^*\mathbf{v}), \qquad [2]$$

with p the pressure, η the shear viscosity, ω the spin field, $\Omega = (\nabla\times\mathbf{v})\cdot\hat{\mathbf{z}}$ the vorticity, $\boldsymbol{\epsilon}$ the Levi–Civita tensor, and $\mathbf{v}^* = \boldsymbol{\epsilon}\cdot\mathbf{v}$. In the stress tensor, the third term refers to the antisymmetric frictional stress that couples the spin to the flow via the rotational viscosity η_R, and the last term to the stress contributed by the dissipationless odd viscosity η_o that produces a stress normal to a shear flow. The angular momentum conservation is described as

$$I(\partial_t + \mathbf{v}\cdot\nabla)\omega = -\Gamma_r\omega - 2\eta_R(2\omega - \Omega) + D\nabla^2\omega + \tau, \qquad [3]$$

with I the moment-of-inertia density, $\Gamma_r = \gamma_r n$ the rotational friction coefficient from environment, $\tau = T_d n$ the torque density, and D the translational diffusion coefficient that is negligible due to the semidilute condition.

From Eqs. **1–3**, together with $\nabla\cdot\mathbf{v} = 0$ and for low Reynolds numbers, the steady-state Stokes-type equation reads

$$0 = -\nabla p + \eta'\nabla^2\mathbf{v} + \eta_o\nabla\Omega - \Gamma\mathbf{v} + \mathbf{g}, \qquad [4]$$

with $\eta' = \eta + \frac{\eta_R\Gamma_r}{\Gamma_r + 4\eta_R}$. This steady-state equation in a polar coordinate system, $\mathbf{v} = v_r\hat{\mathbf{e}}_r + v_\varphi\hat{\mathbf{e}}_\varphi$, needs to be solved with the following hydrodynamic boundary conditions: 1) $\sigma_{\varphi r}|_{r=R} = \eta(2\frac{\partial_\varphi v_r}{r} - 2\frac{v_\varphi}{r} + \Omega) - \eta_R(2\omega - \Omega) - 2\eta_o\partial_r v_r = 0$ (tangential stress vanishing on the frictionless obstacle surface, $R = \sigma_s$), 2) $v_r|_{r=R} = 0$, and 3) $\mathbf{v}|_{r=\infty} = \mathbf{g}/\Gamma$.

To obtain the velocity field of the chiral active fluid, the Stokes equation is simplified using its linearity. The solution of the present equations is a linear superposition of solutions of two simpler problems: 1) the fluid subjected only to the torque τ and

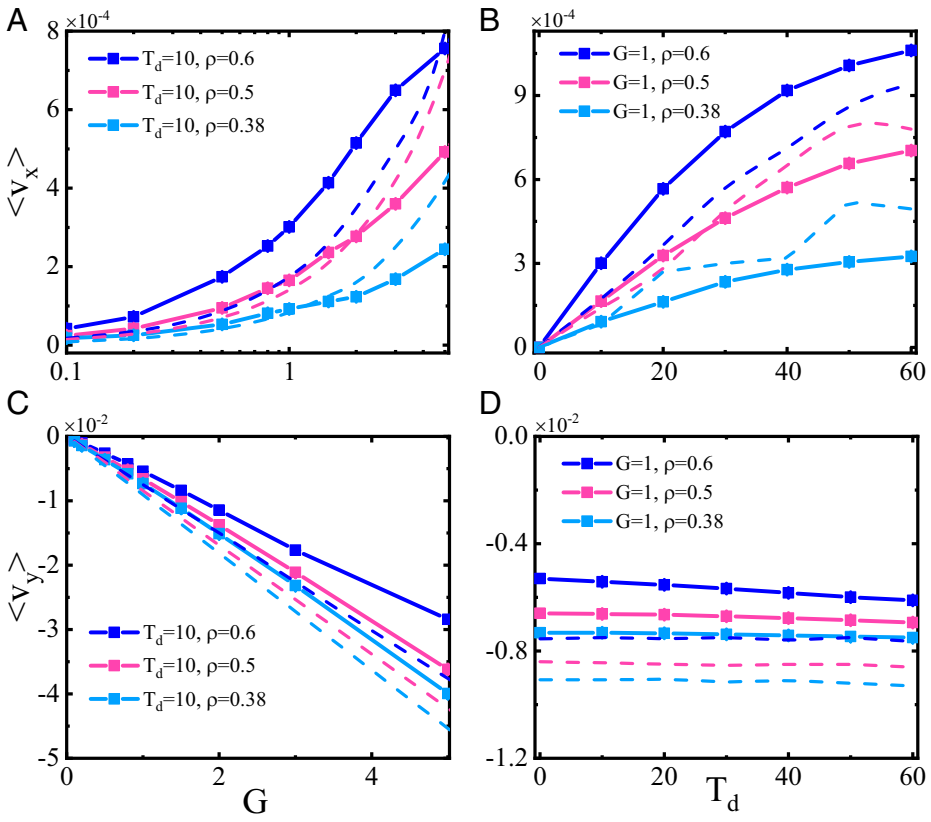

Fig. 2. (*A* and *B*) Transverse Hall-like velocity of spinner fluid crossing a square lattice matrix of obstacles as a function of (*A*) the external force with $T_d = 10$ and (*B*) the driving torque with $G = 1$, for three different spinner packing fractions. (*C* and *D*) The corresponding longitudinal flow velocity as a function of (*C*) G and (*D*) T_d. The symbols and dashed lines correspond to the simulation results and theoretical predictions, respectively.

2) the fluid subjected only to the driving force $\mathbf{g}$. Thus, from Eq. **4**, together with the boundary conditions, a lengthy calculation (see *SI Appendix* for the full theoretical derivation) yields the steady-state velocity field

$$v_r = -\frac{g}{\Gamma}\left(1 + \frac{E_0}{r'^2} - C_0\delta^2\frac{\mathrm{K}_1(r')}{r'}\right)\sin(\varphi) + \frac{g}{\Gamma}\left(\frac{W_0}{r'^2} - D_0\delta^2\frac{\mathrm{K}_1(r')}{r'}\right)\cos(\varphi), \quad [5]$$

$$v_\varphi = F_0\tau\mathrm{K}_1(r') - \frac{g}{\Gamma}\left(1 - \frac{E_0}{r'^2} - C_0\delta^2\mathrm{K}_1'(r')\right)\cos(\varphi) + \frac{g}{\Gamma}\left(\frac{W_0}{r'^2} + D_0\delta^2\mathrm{K}_1'(r')\right)\sin(\varphi). \quad [6]$$

Here, $g = |\mathbf{g}|$, $\delta^2 = \eta'/\Gamma$, $\mathrm{K}_1(r')$ is the first-order Hankel function of imaginary argument with $r' = r/\delta$, and $\mathrm{K}_1'(r') = \partial\mathrm{K}_1/\partial r'$. The definitions of the coefficients C_0, D_0, E_0, F_0, and W_0 (which depend on the viscosities, the friction coefficient,

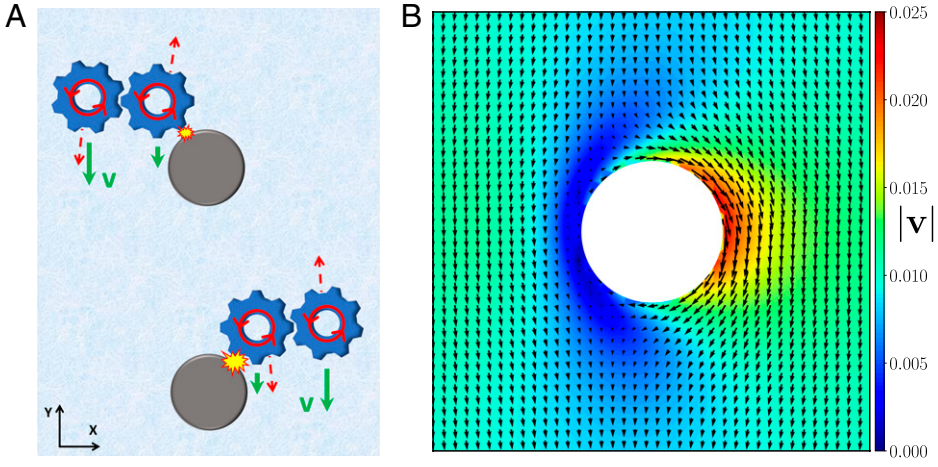

Fig. 3. (*A*) Sketch of a microscopic explanation of the transverse transport of the spinner fluid passing frictionless obstacles. The upper left and lower right parts respectively correspond to the interspinner collisions occurring on the left and right upper sides of the obstacle. The green arrow represents the local longitudinal flow velocity, while the red dashed arrow refers to the friction from the interspinner collisions. (*B*) Representative flow field of the incompressible chiral active fluid passing a smooth obstacle. In the calculation, $G = 1.0$, $T_d = 40$, and $\eta_o = -21.5$ correspond to the spinner fluid of $\rho = 0.6$ in the simulation. The color bars represent the velocity magnitude, and the middle white circle is the obstacle.

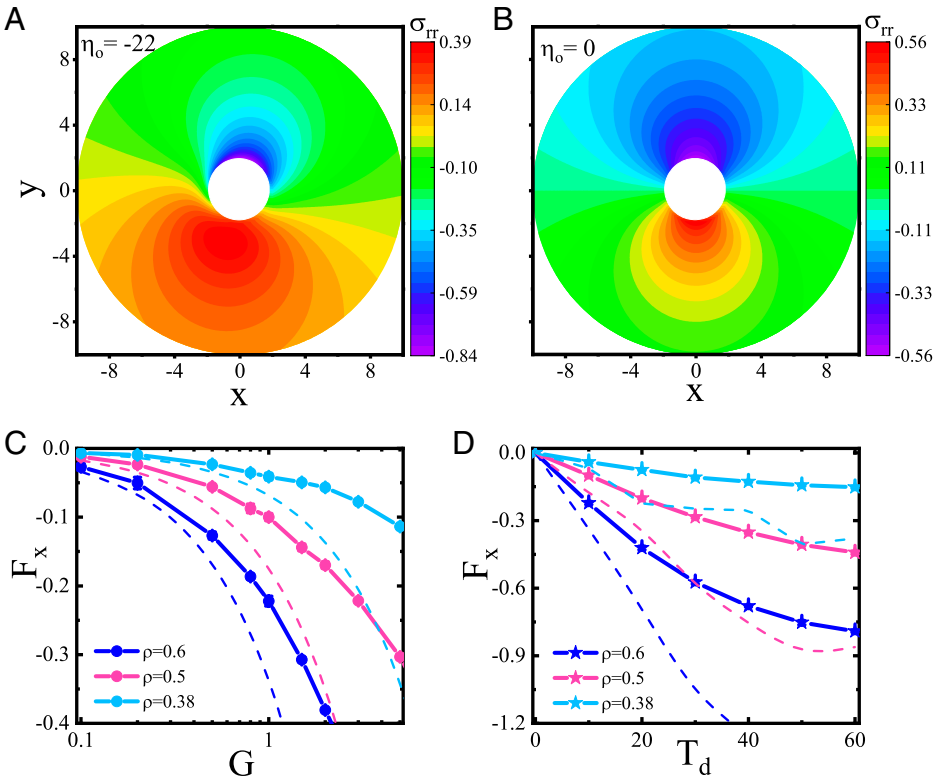

Fig. 4. (*A* and *B*) Theoretical radial stress distribution of the chiral active fluid across a smooth obstacle with (*A*) and without (*B*) the odd viscosity. Here, $\rho = 0.6$, $T_d = 40$, $G = 1$, and the constant hydrostatic pressure p_0 is omitted. (*C* and *D*) The transverse force on an obstacle in a square lattice matrix with $\rho_{ob} = 0.074$ exerted by the spinner fluid as a function of (*C*) G with $T_d = 10$ and (D) T_d with $G = 1$. The symbols and dashed lines refer to the simulation and theory (Eq. **8**), respectively.

and R) are presented in *SI Appendix*. The coefficients have the following important features: C_0 and E_0 are even functions of η_o, while D_0 and W_0 are odd; while F_0 is independent of η_o. From Eqs. **5** and **6** with the viscosities determined by independent simulations (*SI Appendix*), the velocity field of the spinner fluid passing a smooth obstacle is directly determined, as plotted in Fig. 3*B*.

Furthermore, we calculate the mean transverse and longitudinal velocities of the spinners through a square matrix of obstacles, by averaging the analytic velocity field (Eqs. **5** and **6**) around the single obstacle over a square region that exactly corresponds to the elementary cell of the obstacle matrix in the simulation (see *SI Appendix* for the details). In this calculation, we have implicitly assumed that the flow fields around different obstacles in the simulation are independent, as the influence of obstacles on the driving longitudinal flow decays fast due to the strong environmental friction. Fig. 2 indicates that the theoretical calculations are fully consistent with the simulations.

By inserting the flow velocity Eqs. **5** and **6** into Eq. **4**, we obtain the steady-state pressure

$$p = \frac{W_0\cos(\varphi) - E_0\sin(\varphi)}{r'}\delta g + \eta_o\Omega + p_0, \qquad [7]$$

with p_0 the pressure at infinity. Due to the frictionless obstacle, the transverse flow is generated only by the radial stress, $\sigma_{rr} = -p - 2\eta_o(\frac{v_\varphi}{r} - \frac{\partial_\varphi v_r}{r} - \frac{\Omega}{2}) + 2\eta\partial_r v_r$, and the radial stress distribution can be straightforwardly calculated by substituting Eqs. **5**–**7** into σ_{rr}, as plotted in Fig. 4 *A* and *B*. The result indicates that the existence of the odd viscosity leads to an asymmetry of the radial stress distribution with respect to the y axis across the obstacle center, which is absent for $\eta_o = 0$. It is the asymmetric radial stress that generates the Hall-like transport. Furthermore, by integrating the radial stress over the obstacle surface, the transverse force on the obstacle exerted by the spinner fluid is obtained as

$$F_x = -\pi\delta^2 W_0 g + 2\pi\eta_o g\left(\frac{\mathrm{K}_2(R')\delta^2 C_0}{\Gamma} - \frac{2E_0}{\Gamma R'^2}\right) + 2\pi\eta g\left(\frac{\mathrm{K}_2(R')\delta^2 D_0}{\Gamma} - \frac{2W_0}{\Gamma R'^2}\right), \qquad [8]$$

with $R' = R/\delta$. The reaction force to F_x is then just the driving force of the transverse Hall-like flow and vanishes when $\mathbf{g} = 0$ or $\eta_o = 0$, as the coefficients D_0 and W_0 are zero for $\eta_o = 0$ (no matter what the values of η and η_R are). The reversal of $\langle v_x\rangle$ for the clockwise spinners (opposite η_o) arises from the fact that D_0 and W_0 are odd functions of η_o, while C_0 and E_0 are even. The semiquantitative agreement between F_x obtained by simulation and predicted from Eq. **8** (Fig. 4 *C* and *D*) implies that the odd viscosity is essential for the Hall-like transport.

Although the hydrodynamic theory properly captures the essential features of the Hall-like transport of the spinner fluid, it contains several important approximations: First, the discrete spinner system is regarded as a continuum fluid; second, the compressible spinner fluid is assumed to be incompressible; third, the inertial term is not taken into account; and last but not least, the correlations of spinner density and flow velocity induced by multiple obstacles are neglected owing to the strong environment friction. These approximations constitute the main sources of the quantitative difference between the theory and simulation. Particularly, the compressibility and the inertial effect both increase with the external driving force. In addition, due to the flow correlation, the upper obstacles in the matrix can effectively screen the lower ones from the longitudinal flow, which also becomes prominent

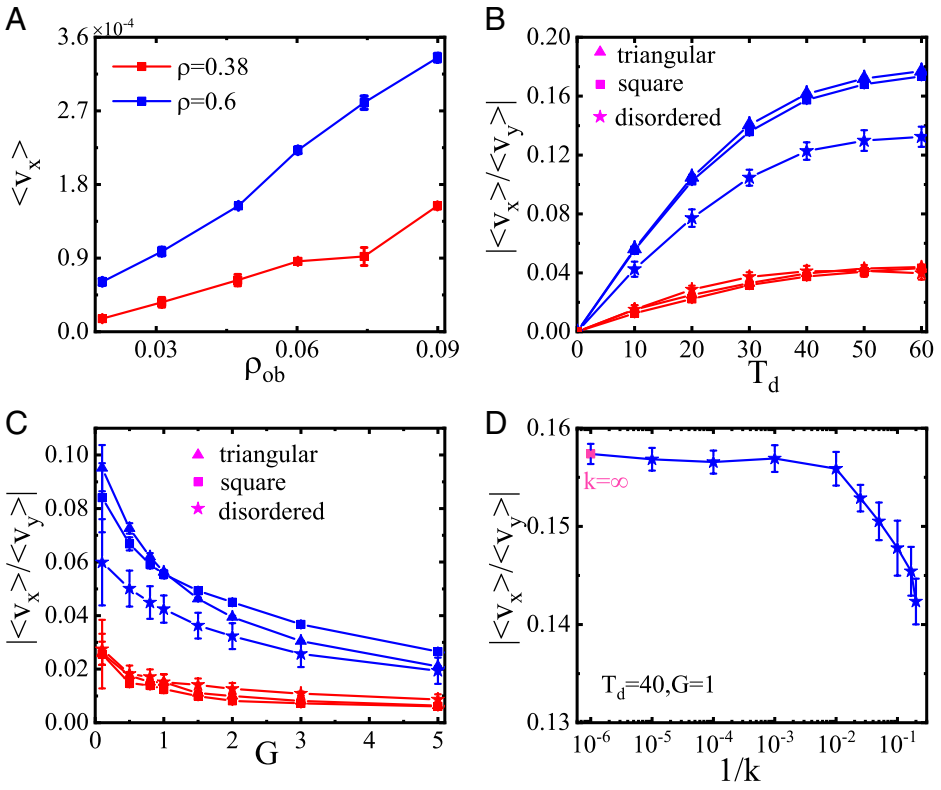

Fig. 5. (*A*) Transverse velocity of the spinners as a function of the packing fraction of the obstacles on a square lattice, with $G = 1$ and $T_d = 10$. (*B* and *C*) The ratio of the transverse to longitudinal flow velocities as a function of (*B*) T_d with $G = 1$ and (*C*) G with $T_d = 10$, in the square (squares), triangular (triangles), and disordered (stars) matrices. Here, for disordered obstacles, 16 different matrix configurations were used for averaging the flow velocity. (*D*) The ratio of the transverse to longitudinal velocities versus the degree of disordered deviation from the perfect square lattice, with $T_d = 40$ and $G = 1$. In *B*–*D*, $\rho_{ob} = 0.074$ remains fixed. The blue and red symbols correspond to $\rho = 0.6$ and 0.38, respectively.

for larger G. Consequently, the hydrodynamic theory is expected to be more appropriate for smaller G.

C. Obstacle Matrix Effects. We now investigate the effect of the impurity packing fraction on the transverse flow in the square matrix, keeping the spinner packing fraction unchanged (with respect to the obstacle free space). Fig. 5*A* shows that the transverse velocity significantly increases with ρ_{ob} in the dilute or semidilute regime. This is simply because more obstacles can result in more fluid regions subjected to a local nonuniform shear and hence larger transverse driving force.

Further, we consider different matrix structures, including a triangular lattice matrix and a disordered matrix (constructed by randomly placing the obstacles in the simulation box with the interobstacle separation larger than $2\sigma_s$). The ordered or disordered matrix may generally mimic the impurity background in electronic anomalous Hall systems. To better manifest the efficiency of the Hall-like transport in different matrices, Fig. 5 *B* and *C* plots the ratio of the transverse to longitudinal flow velocities (corresponding to the Hall angle). All matrix types invariably exhibit a significant Hall-like flux along the x axis, implying that the detailed nature of the impurity matrix is not essential for the emergence of the transverse transport. As long as there are frozen impurities creating a local shear in the spinner fluid, the odd viscosity will generate a nonzero transverse flow, thus constituting a very robust effect. Nevertheless, the matrix structure indeed has a quantitative influence on the magnitude of the Hall-like transport. From Fig. 5 *B* and *C*, it is clear that for low ρ the Hall-like transport hardly depends on the matrix structure, since in the dilute fluid, having low viscosities, the correlations of velocities and densities induced by neighboring obstacles are weak. While, for high ρ, the Hall-like transport in the disordered matrix is weaker than those in the square and triangle lattices. It can be reasonably speculated that in the dense fluid with high viscosities, the velocity field and density distribution around neighboring obstacles strongly correlate, so that different obstacle structures could have different transport efficiencies. Comparing with the periodic ordered lattices, the obstacles in the disordered matrix are randomly distributed in space, where local dense regions of obstacles strongly hinder the spinner flow while local dilute regions cannot effectively shear the spinner longitudinal flow. As a result, such local dense and dilute regions in the disordered matrix are adverse to driving the transverse transport.

Furthermore, to study the dependence of the velocity ratio on the degree of disorder of the obstacle matrix, we construct the matrices by randomly quenching the fluctuating obstacles that are constrained to a perfect square lattice through a harmonic spring potential with a spring constant k. In this situation, the degree of disorder of the obstacle matrix increases with reducing k. The simulation result in Fig. 5*D* indicates that the Hall-like transport weakens as the degree of disorder increases, which is consistent with the above speculation.

D. Compressibility Effects and Antisymmetric Stress. The hydrodynamic calculation shows that the Hall-like transport of the incompressible spinner fluid originates exclusively from the odd viscosity. Nevertheless, the spinner fluid in the simulation is not strictly incompressible, so that its density distribution is nonuniform around the obstacle. In this case, the antisymmetric stress from the rotational viscosity (density dependent), $\eta_R(r)\epsilon(2\omega - \Omega)$, induces nonsymmetric edge flows at the top and bottom surfaces of the obstacle (31), thus seemingly also

causing a transverse flow. However, it can be shown that the position-dependent antisymmetric stress does not contribute to the transverse driving force even in a compressible spinner fluid, since the tangential stress vanishes at the surface of the frictionless obstacle [$\sigma_{\varphi r}(R) = 0$] and the antisymmetric stress occurs only in $\sigma_{\varphi r}$. On the other hand, for a rough obstacle with a no-slip boundary, the tangential stress is nonzero at the obstacle surface, such that $\eta_R(r)\epsilon(2\omega - \Omega)$ does play a role and contributes to a transverse force, actually overwhelming the contribution from the odd viscosity, as demonstrated by the simulation of the rough obstacles in *SI Appendix*.

We also point out that although the compressibility does not play a fundamental role for the emergence of the Hall-like transport, it does quantitatively affect the transverse flow, as shown by the simulations with softer interparticle steric repulsions (*SI Appendix*).

Discussion

Similarity with Anomalous Hall Effect. Besides the edge flow, odd viscosity, and spin–spin and spin–orbital couplings, the emergence of transverse transport without magnetic field further strengthens the similarity between the active spinner fluid and the electronic anomalous Hall systems. Particularly, based on the hydrodynamic framework developed for correlated electron systems (48, 54, 55), it may establish a possible mapping between the present finding and the anomalous Hall effect.

For a 2D anomalous Hall system with the magnetization $\mathbf{M}$, the hydrodynamic theory (55) includes two different terms that can give rise to the transverse flow: $\sim\mathbf{v} \times \mathbf{M}$ and $\eta_o \nabla^2 \mathbf{v} \times \mathbf{z}$. The former is analogous to the common Lorentz force ($\mathbf{M}$ corresponds to an effective magnetic field), which plays a universal role; while the latter is exactly equal to the odd viscosity term in the active spinner fluid. Therefore, in the hydrodynamic framework the odd viscosity term connects the transverse transport of the chiral active fluid to the anomalous Hall effect. In 2D systems, the odd viscosity arises from the breaking of time-reversal and parity symmetries, which are induced separately by the magnetization in anomalous Hall systems (magnetic field in normal Hall systems) and by the particle spin in the active spinner fluid. In this sense, the self-driven torque field corresponds to an effective magnetic field in the chiral active fluid. Moreover, the odd viscosity increases separately with the magnetic field in the Hall system, while increasing conjointly with the spin angular velocity in the spinner fluid, further strengthening the correspondence between the self-driven torque field and the effective magnetic field.

Besides the absence of the Lorentz-type force, another important difference between the Hall effect and the transverse transport of the spinner fluid lies in the nature of the environment where the odd viscosity term plays a role. In electronic Hall systems, the odd viscosity usually contributes to the Hall flow near the no-slip–like channel walls, where the longitudinal flow is inhomogeneous, rather than around the quenched frictionless impurities. While, for the chiral active fluid, the odd viscosity plays a role both around the microscopic obstacles and near the system boundary walls (*SI Appendix*).

Comparison with Transverse Motion in Other Systems Due to Odd Viscosity. The charge-neutral confined polyatomic gases under an external magnetic field also exhibit transverse transport due to the odd viscosity (56, 57). However, one should bear in mind that the polyatomic gases are fundamentally different from the present chiral active fluid in the following aspects: First, the transverse flow of the polyatomic gases needs an external magnetic field, similar to the normal Hall effect, in stark contrast to the case of the chiral active fluid. Second, the spinner fluid is active; while the polyatomic gases are passive systems, where the gas molecule does not experience any self-propulsion. Third, in the polyatomic gases, the transverse force is generated by the no-slip boundary walls of the channel instead of the frictionless impurities with a size comparable to the particle. And finally, the odd viscosity of the polyatomic gas is very small, with the ratio of the odd to shear viscosities $\eta_o/\eta \sim 0.001$; while $\eta_o/\eta \sim 1$ in the spinner fluid, so that the active spinner fluid may exhibit a Hall-like transport orders of magnitude stronger than the passive polyatomic gases.

A very recent theoretical work (58) predicts that a no-slip passive disk, moving laterally in a quasi-2D compressible traditional fluid with an assumed odd viscosity, experiences a lift force that vanishes in the incompressible limit. This prediction does not contradict our results, since the quenched obstacles in our system are frictionless. Additionally, it would be interesting to study also the odd viscosity effect on the circle swimmer transport, even if the circle swimmer system does appear to be more complex than the spinner fluid because of the self-propelled translation (15, 59). Even an isolated circle swimmer experiences a transverse rectification in a symmetric potential (60). Such a single-particle effect may also be the main reason for the transverse motion of a passive probe driven through a circle swimmer fluid (61). Therefore, identifying the odd viscosity contribution, if any, to the transport in circle swimmer systems remains an open question.

Conclusion

Active spinner fluid exhibits an anomalous Hall-like effect when it is driven to flow through a matrix of obstacles. The transverse mass transport arises exclusively from the odd viscosity effect in the spinner fluid under local nonuniform shear. This finding extends also our understanding of the role of odd viscosity in electronic Hall systems, where it corrects only the Hall conductance (38, 48–51, 53, 55). Our results thus highlight the fundamental importance of odd viscosity in active chiral matter and are experimentally verifiable by using colloidal spinners or macroscopic granular spinners.

Data, Materials, and Software Availability. All study data are included in the article and/or *SI Appendix*.

ACKNOWLEDGMENTS. We thank N. Zheng, C. M. Wang, and R. Liu for helpful discussions. We acknowledge the support of the National Natural Science Foundation of China (11874397, 11674365, and 11774394), the Key Research Program of Frontier Sciences of the Chinese Academy of Sciences (12034019), and the Strategic Priority Research Program of the Chinese Academy of Sciences (XDB33000000).

Author affiliations: [a]School of Physical Sciences, University of Chinese Academy of Sciences, Beijing 100049, China; [b]Beijing National Laboratory for Condensed Matter Physics, Institute of Physics, Chinese Academy of Sciences, Beijing 100190, China; [c]Laboratory of Soft Matter Physics, Institute of Physics, Chinese Academy of Sciences, Beijing 100190, China; [d]Wenzhou Institute, University of Chinese Academy of Sciences, Wenzhou 325001, China; [e]Songshan Lake Materials Laboratory, Dongguan 523808, China; and [f]Kavli Institute for Theoretical Sciences, University of Chinese Academy of Sciences, Beijing 100049, China

1. J. Elgeti, R. G. Winkler, G. Gompper, Physics of microswimmers–single particle motion and collective behavior: A review. *Rep. Prog. Phys.* **78**, 056601 (2015).
2. T. Markovich, E. Tjhung, M. E. Cates, Chiral active matter: Microscopic 'torque dipoles' have more than one hydrodynamic description. *New J. Phys.* **21**, 112001 (2019).
3. H. Noji, R. Yasuda, M. Yoshida, K. Kinosita Jr., Direct observation of the rotation of F1-ATPase. *Nature* **386**, 299–302 (1997).
4. I. H. Riedel, K. Kruse, J. Howard, A self-organized vortex array of hydrodynamically entrained sperm cells. *Science* **309**, 300–303 (2005).

5. B. M. Friedrich, F. Jülicher, Chemotaxis of sperm cells. *Proc. Natl. Acad. Sci. U.S.A.* **104**, 13256–13261 (2007).
6. R. Di Leonardo, D. Dell'Arciprete, L. Angelani, V. Iebba, Swimming with an image. *Phys. Rev. Lett.* **106**, 038101 (2011).
7. A. P. Petroff, X. L. Wu, A. Libchaber, Fast-moving bacteria self-organize into active two-dimensional crystals of rotating cells. *Phys. Rev. Lett.* **114**, 158102 (2015).
8. X. Chen, X. Yang, M. Yang, H. P. Zhang, Dynamic clustering in suspension of motile bacteria. *Europhys. Lett.* **111**, 54002 (2015).
9. J. M. Catchmark, S. Subramanian, A. Sen, Directed rotational motion of microscale objects using interfacial tension gradients continually generated via catalytic reactions. *Small* **1**, 202–206 (2005).
10. S. Ebbens, R. A. Jones, A. J. Ryan, R. Golestanian, J. R. Howse, Self-assembled autonomous runners and tumblers. *Phys. Rev. E Stat. Nonlin. Soft Matter Phys.* **82**, 015304 (2010).
11. N. H. P. Nguyen, D. Klotsa, M. Engel, S. C. Glotzer, Emergent collective phenomena in a mixture of hard shapes through active rotation. *Phys. Rev. Lett.* **112**, 075701 (2014).
12. M. Yang, M. Ripoll, A self-propelled thermophoretic microgear. *Soft Matter* **10**, 1006–1011 (2014).
13. M. Yang, M. Ripoll, K. Chen, Catalytic microrotor driven by geometrical asymmetry. *J. Chem. Phys.* **142**, 054902 (2015).
14. C. Maggi, F. Saglimbeni, M. Dipalo, F. De Angelis, R. Di Leonardo, Micromotors with asymmetric shape that efficiently convert light into work by thermocapillary effects. *Nat. Commun.* **6**, 7855 (2015).
15. F. Kümmel *et al.*, Circular motion of asymmetric self-propelling particles. *Phys. Rev. Lett.* **110**, 198302 (2013).
16. G. Kokot *et al.*, Active turbulence in a gas of self-assembled spinners. *Proc. Natl. Acad. Sci. U.S.A.* **114**, 12870–12875 (2017).
17. M. Han, J. Yan, S. Granick, E. Luijten, Effective temperature concept evaluated in an active colloid mixture. *Proc. Natl. Acad. Sci. U.S.A.* **114**, 7513–7518 (2017).
18. H. Massana-Cid, D. Levis, R. Hernández, I. Pagonabarraga, P. Tierno, Arrested phase separation in chiral fluids of colloidal spinners. *Phys. Rev. Res.* **3**, L042021 (2021).
19. C. Scholz, M. Engel, T. Pöschel, Rotating robots move collectively and self-organize. *Nat. Commun.* **9**, 1–8 (2018).
20. J. C. Tsai, F. Ye, J. Rodriguez, J. P. Gollub, T. C. Lubensky, A chiral granular gas. *Phys. Rev. Lett.* **94**, 214301 (2005).
21. X. Yang, C. Ren, K. Cheng, H. P. Zhang, Robust boundary flow in chiral active fluid. *Phys. Rev. E* **101**, 022603 (2020).
22. P. Liu *et al.*, Oscillating collective motion of active rotors in confinement. *Proc. Natl. Acad. Sci. U.S.A.* **117**, 11901–11907 (2020).
23. B. C. van Zuiden, J. Paulose, W. T. M. Irvine, D. Bartolo, V. Vitelli, Spatiotemporal order and emergent edge currents in active spinner materials. *Proc. Natl. Acad. Sci. U.S.A.* **113**, 12919–12924 (2016).
24. K. Dasbiswas, K. K. Mandadapu, S. Vaikuntanathan, Topological localization in out-of-equilibrium dissipative systems. *Proc. Natl. Acad. Sci. U.S.A.* **115**, E9031–E9040 (2018).
25. D. Banerjee, A. Souslov, A. G. Abanov, V. Vitelli, Odd viscosity in chiral active fluids. *Nat. Commun.* **8**, 1573 (2017).
26. V. Soni *et al.*, The odd free surface flows of a colloidal chiral fluid. *Nat. Phys.* **15**, 1188–1194 (2019).
27. Z. Liao, M. Han, M. Fruchart, V. Vitelli, S. Vaikuntanathan, A mechanism for anomalous transport in chiral active liquids. *J. Chem. Phys.* **151**, 194108 (2019).
28. C. Hargus, K. Klymko, J. M. Epstein, K. K. Mandadapu, Time reversal symmetry breaking and odd viscosity in active fluids: Green-Kubo and NEMD results. *J. Chem. Phys.* **152**, 201102 (2020).
29. T. Markovich, T. C. Lubensky, Odd viscosity in active matter: Microscopic origin and 3d effects. *Phys. Rev. Lett.* **127**, 048001 (2021).
30. M. Han *et al.*, Fluctuating hydrodynamics of chiral active fluids. *Nat. Phys.* **17**, 1260–1269 (2021).
31. Q. Yang *et al.*, Topologically protected transport of cargo in a chiral active fluid aided by odd-viscosity-enhanced depletion interactions. *Phys. Rev. Lett.* **126**, 198001 (2021).
32. K. v. Klitzing, G. Dorda, M. Pepper, New method for high-accuracy determination of the fine-structure constant based on quantized Hall resistance. *Phys. Rev. Lett.* **45**, 494–497 (1980).
33. D. J. Thouless, M. Kohmoto, M. P. Nightingale, M. den Nijs, Quantized Hall conductance in a two-dimensional periodic potential. *Phys. Rev. Lett.* **49**, 405–408 (1982).
34. X. L. Qi, S. C. Zhang, Topological insulators and superconductors. *Rev. Mod. Phys.* **83**, 175–179 (2010).
35. M. Z. Hasan, C. L. Kane, Colloquium: Topological insulators. *Rev. Mod. Phys.* **82**, 3045–3067 (2010).
36. J. E. Avron, R. Seiler, P. G. Zograf, Viscosity of quantum Hall fluids. *Phys. Rev. Lett.* **75**, 697–700 (1995).
37. N. Read, Non-Abelian adiabatic statistics and Hall viscosity in quantum Hall states and $p_x + ip_y$ paired superfluids. *Phys. Rev. B Condens. Matter Mater. Phys.* **79**, 045308 (2009).
38. C. Hoyos, D. T. Son, Hall viscosity and electromagnetic response. *Phys. Rev. Lett.* **108**, 066805 (2012).
39. F. D. M. Haldane, Model for a quantum Hall effect without Landau levels: Condensed-matter realization of the "parity anomaly". *Phys. Rev. Lett.* **61**, 2015–2018 (1988).
40. C. Z. Chang *et al.*, Experimental observation of the quantum anomalous Hall effect in a magnetic topological insulator. *Science* **340**, 167–170 (2013).
41. H. Weng, R. Yu, X. Hu, X. Dai, Z. Fang, Quantum anomalous Hall effect and related topological electronic states. *Adv. Phys.* **64**, 227–282 (2015).
42. C. X. Liu, S. C. Zhang, X. L. Qi, The quantum anomalous Hall effect: Theory and experiment. *Annu. Rev. Condens. Matter Phys.* **7**, 301–321 (2016).
43. N. Nagaosa, J. Sinova, S. Onoda, A. H. MacDonald, N. P. Ong, Anomalous Hall effect. *Rev. Mod. Phys.* **82**, 1539–1592 (2010).
44. E. Hall, On the possibility of transvers currents in ferromagnets. *Philos. Mag.* **12**, 157–172 (1881).
45. M. P. Allen, D. J. Tildesley, *Computer Simulation of Liquids* (Oxford University Press, 2017).
46. J. E. Avron, Odd viscosity . *J. Stat. Phys.* **92**, 543–557 (1998).
47. S. Ganeshan, A. G. Abanov, Odd viscosity in two-dimensional incompressible fluids. *Phys. Rev. Fluids* **2**, 094101 (2017).
48. T. Scaffidi, N. Nandi, B. Schmidt, A. P. Mackenzie, J. E. Moore, Hydrodynamic electron flow and Hall viscosity. *Phys. Rev. Lett.* **118**, 226601 (2017).
49. L. V. Delacrétaz, A. Gromov, Transport signatures of the Hall viscosity. *Phys. Rev. Lett.* **119**, 226602 (2017).
50. T. Holder, R. Queiroz, A. Stern, Unified description of the classical Hall viscosity. *Phys. Rev. Lett.* **123**, 106801 (2019).
51. A. I. Berdyugin *et al.*, Measuring Hall viscosity of graphene's electron fluid. *Science* **364**, 162–165 (2019).
52. Y. You, E. Fradkin, Field theory of nematicity in the spontaneous quantum anomalous Hall effect. *Phys. Rev. B* **88**, 235124 (2013).
53. A. Cortijo, Y. Ferreirós, K. Landsteiner, M. A. Vozmediano, Visco elasticity in 2D materials. *2D Materials* **3**, 011002 (2016).
54. P. S. Alekseev, Negative magnetoresistance in viscous flow of two-dimensional electrons. *Phys. Rev. Lett.* **117**, 166601 (2016).
55. H. Funaki, R. Toshio, G. Tatara, Vorticity-induced anomalous Hall effect in an electron fluid. *Phys. Rev. Res.* **3**, 033075 (2021).
56. J. Korving, H. Hulsman, H. F. P. Knaap, J. J. M. Beenakker, Transverse momentum transport in viscous flow of diatomic gases in a magnetic field. *Phys. Lett.* **21**, 5–7 (1966).
57. H. Hulsman, E. J. Van Waasdijk, A. L. J. Burgmans, H. F. P. Knaap, J. J. M. Beenakker, Transverse momentum transport in polyatomic gases under the influence of a magnetic field. *Physica* **50**, 53–76 (1970).
58. Y. Hosaka, S. Komura, D. Andelman, Nonreciprocal response of a two-dimensional fluid with odd viscosity. *Phys. Rev. E* **103**, 042610 (2021).
59. M. Huang, W. Hu, S. Yang, Q. X. Liu, H. P. Zhang, Circular swimming motility and disordered hyperuniform state in an algae system. *Proc. Natl. Acad. Sci. U.S.A.* **118**, e2100493118 (2021).
60. J. Wu, J. Zhou, B. Ai, Transport reversals of chiral active particles induced by a perpendicular constant force. *Physica A* **462**, 864–869 (2016).
61. C. Reichhardt, C. J. O. Reichhardt, Active microrheology, Hall effect, and jamming in chiral fluids. *Phys. Rev. E* **100**, 012604 (2019).